# Phase equilibrium of $Cd_{1-x}Zn_xS$ alloys studied by first-principles calculations and Monte Carlo simulations*

Fu-Zhen Zhang(张付珍)[1], Hong-Tao Xue(薛红涛)[1,†], Fu-Ling Tang(汤富领)[1,‡], Xiao-Kang Li(李小康)[1], Wen-Jiang Lu(路文江)[1], and Yu-Dong Feng(冯煜东)[2]

[1] *State Key Laboratory of Advanced Processing and Recycling of Nonferrous Metals, Department of Materials Science and Engineering, Lanzhou University of Technology, Lanzhou 730050, China*

[2] *Science and Technology on Surface Engineering Laboratory, Lanzhou Institute of Physics, Lanzhou 730000, China*

(Received 23 June 2015; revised manuscript received 13 September 2015; published online 30 November 2015)

The first-principles calculations based on density functional theory combined with cluster expansion techniques and Monte Carlo (MC) simulations were used to study the phase diagrams of both wurtzite (WZ) and zinc-blende (ZB) $Cd_{1-x}Zn_xS$ alloys. All formation energies are positive for WZ and ZB $Cd_{1-x}Zn_xS$ alloys, which means that the $Cd_{1-x}Zn_xS$ alloys are unstable and have a tendency to phase separation. For WZ and ZB $Cd_{1-x}Zn_xS$ alloys, the consolute temperatures are 655 K and 604 K, respectively, and they both have an asymmetric miscibility gap. We obtained the spatial distributions of Cd and Zn atoms in WZ and ZB $Cd_{0.5}Zn_{0.5}S$ alloys at different temperatures by MC simulations. We found that both WZ and ZB phases of $Cd_{0.5}Zn_{0.5}S$ alloy exhibit phase segregation of Cd and Zn atoms at low temperature, which is consistent with the phase diagrams.

**Keywords:** first-principles calculation, Monte Carlo simulations, phase separation, spatial distribution

**PACS:** 31.15.A–, 64.75.–g, 64.75.Qr, 63.70.+h **DOI:** 10.1088/1674-1056/25/1/013103

## 1. Introduction

Both CdS and ZnS are II–VI direct band gap semiconductors, and their band gaps are 2.40 eV and 3.65 eV, respectively.[1–3] The former is a typical material for the buffer layer of the high-efficiency $CuIn_{1-x}Ga_xSe_2$ thin film solar cells.[4] However, cadmium, a kind of heavy metal toxic element, can do harm to the environment and human health. To reduce the cadmium usage as well as to improve the optical and electronic properties of the buffer layer, one feasible way is to replace CdS by $Cd_{1-x}Zn_xS$ solid solution. The band gap and light transmission of CdS can be improved by doping with Zn.[5–7]

To date, the $Cd_{1-x}Zn_xS$ alloys have been widely studied both experimentally and theoretically. In experiments, researchers mainly focused on the methods to synthesize $Cd_{1-x}Zn_xS$ alloys. For example, many methods, such as the chemical co-precipitation method,[8,9] chemical bath deposition (CBD),[10–13] chemical vapor deposition,[14] molecular beam epitaxy (MBE),[15] solution growth technique (SGT),[16] true liquid crystalline templating (TLCT),[17] precipitate-hydrothermal method,[18,19] and solvothermal route, have been proposed.[20] In addition, there are also many theoretical studies about the properties of $Cd_{1-x}Zn_xS$ solid solutions. Jiao *et al.*[21] studied the structural, electronic, and optical properties of zinc-blende $Zn_{1-x}Cd_xS$ and $ZnS_{1-y}Se_y$ alloys. They predicted that $Zn_{1-x}Cd_xS$ and $ZnS_{1-y}Se_y$ alloys are promising materials for solar cells, photoconductors, and electroluminescent devices due to the materials' high absorption of solar radiation and photoconductivity in the energy region from visible light to ultraviolet. Wan *et al.*[22] calculated the crystal structure and thermal properties of $Cd_{1-x}Zn_xS$ alloys at different temperatures. They found that the lattice parameters decrease with the increase of the Zn concentration. Both the specific heat of constant volume and the coefficient of thermal expansion of $Cd_{1-x}Zn_xS$ increase and saturate as the temperature increases. Wu *et al.*[23] studied the band gaps, band edges, and electronic properties of both wurtzite (WZ) and zinc-blende (ZB) $Cd_{1-x}Zn_xS$ solid solutions by using the special quasi-random structures combined with the hybrid density functional theory (DFT) calculations. Lu *et al.*[24] obtained the phase diagram of WZ $Cd_{1-x}Zn_xS$ solid solution by using the regular solution model with a Bragg–Williams approximation for the entropy of mixing. The binodal curve was determined by drawing a common tangent line to the Gibbs free energy at a given temperature, and the spinodal curve was determined as the curve whose second derivative of Gibbs free energy with respect to the Zn concentration, $\partial^2(\Delta G)/\partial x^2$, is zero. In their study, the consolute temperature $T_c$ of $Cd_{1-x}Zn_xS$ solid solution is 613 K. The miscibility gap is asymmetric, showing a deviation toward to the higher $x$ side. Recently, Zhou *et al.*[25] calculated the phase diagrams of WZ and ZB $Cd_{1-x}Zn_xS$ solid solutions by using first-principles calculations combined with

*Project supported by the National Natural Science Foundation of China (Grant Nos. 11164014 and 11364025) and Gansu Science and Technology Pillar Program, China (Grant No. 1204GKCA057).

†Corresponding author. E-mail: xueht987@163.com

‡Corresponding author. E-mail: tfl03@mails.tsinghua.edu.cn

© 2016 Chinese Physical Society and IOP Publishing Ltd 

the regular solution model. They found that the consolute temperature $T_c$ and the consolute concentration $x_c$ are 1278 K and 0.61 for ZB $Cd_{1-x}Zn_xS$ solid solution, and 1017 K and 0.65 for WZ $Cd_{1-x}Zn_xS$ solid solution, respectively. They indicated that the configuration-average method can improve the mixing enthalpy, which explicitly determines the phase stability of the $Cd_{1-x}Zn_xS$ alloys.[26] The $T_c$ of 1017 K is much higher than that of 613 K reported by Lu *et al.*,[24] which is almost impossible according to the phase diagrams of CdS and ZnS and the preparation temperature of the experiment, because the temperature is too high.[11,27,28]

In this study, we perform first-principles calculations combined with the cluster expansion and Monte Carlo simulations to obtain the phase diagrams of WZ and ZB $Cd_{1-x}Zn_xS$ solid solutions. This method has been successfully used to study the phase equilibrium of many other alloy systems,[29–33] while it has not been used to study the phase stability of $Cd_{1-x}Zn_xS$ solid solutions. In order to analyze the phase separation of $Cd_{1-x}Zn_xS$ systems intuitively, we also present the spatial distributions of Cd and Zn atoms in the two structures of $Cd_{0.5}Zn_{0.5}S$ alloys.

## 2. Computational methodology

### 2.1. Cluster expansion

To study the phase equilibrium and ground-state structures of the $Cd_{1-x}Zn_xS$ alloys, it is necessary to compute the total energies of all possible configurations by placing Cd and Zn atoms on $N$ sites of the Bravais lattice. It is almost impossible to obtain the total energies of all possible configurations exhaustively by first-principles, because the number of possible configurations $2^N$ is enormous. The cluster expansion (CE) method constructs an Ising-like Hamiltonian for calculating the energies of different atomic configurations. This method has been illustrated in Refs. [34]–[38] in detail. For $Cd_{1-x}Zn_xS$ alloys, each configuration is described by a set of "spin" occupation variables $\sigma_i$ at $i$ sites of the lattice, and $\sigma_i = +1$ or $-1$ depending on which kind of atoms occupied site $i$.

The CE parameterizes the configurational energy (per exchangeable cation) as a polynomial in "spin" occupation variables

$$E(\sigma) = \sum_{\alpha} m_\alpha J_\alpha \left\langle \prod_{i \in \alpha'} \sigma_i \right\rangle, \tag{1}$$

where $\alpha$ is a cluster (a set of lattice sites). The sum is taken over all clusters $\alpha$ that are not equivalent by a symmetry operation of the space group of the parent lattice, while the average is taken over all clusters $\alpha'$ that are equivalent to $\alpha$ by symmetry. The coefficient $J_\alpha$ is known as the effective cluster interaction (ECI) parameter. The multiplicity $m_\alpha$ stands for the number of clusters that are equivalent to $\alpha$ by symmetry. It is seen that when all clusters $\alpha$ are considered in the sum, the cluster expansion is able to represent the energy $E(\sigma)$ of any configuration $\sigma$ by an appropriate selection of the values of $J_\alpha$. The unknown parameters of the cluster expansion (the ECIs) are then determined by fitting them to the energies of a relatively small number of configurations obtained by first-principles calculations.[39] The CE method was performed with the Alloy Theoretic Automated Toolkit (ATAT), which can automate most of the tasks associated with the construction of the CE Hamiltonian and the calculation of thermodynamic properties.[39–41] ATAT proceeds by gradually increasing the number of clusters included in the cluster expansion until the desired accuracy is achieved.

We introduced the cross-validation (CV) score as the criterion to evaluate the predictive power of the cluster expansion. The CV score is defined as

$$\mathrm{CV} = \left( \frac{1}{n} \sum_{i=1}^{n} \left( E_i - \hat{E}_i \right)^2 \right)^{1/2}, \tag{2}$$

where $E_i$ is the calculated energy of structure $i$, while $\hat{E}_i$ is the predicted energy of structure $i$ obtained from a least-squares fit to the $(n-1)$ other structural energies.[39] When the CV score is small, typically less than 25 meV, we considered it satisfactory. The CV score is an improvement relative to the standard mean square error criterion that only minimizes the error for structures included in the fit and is not monotonically decreasing. The CV score can decrease to a minimum with the increasing number of fitted clusters. This is because an increasing number of degrees of freedom are used to account for the fluctuation in energy. It also can increase when the number of fitted clusters is large, which will reduce the predictive power of CE because of the increase of the noise in the fitted ECIs.[39]

### 2.2. Total energy calculations

The electronic-structure total-energy calculations of ordered structures, which are required for the construction of the cluster expansion Hamiltonian, were performed using the Vienna *ab initio* simulation package (VASP).[42,43] The interaction between the core and the valence electrons was included by the frozen-core projector augmented wave (PAW) method.[44,45] The valence electron configurations for the pseudopotentials are Cd: $4d^{10}5s^2$, Zn: $3d^{10}4s^2$, and S: $3s^23p^4$. Both lattice parameters and ionic positions were fully relaxed for all supercells. The plane-wave energy cutoff was 370 eV. The generalized gradient approximation (GGA) functional of Perdew–Burke–Ernzerhof (PBE) was introduced to describe the exchange–correlation energy.[46] ATAT was used as a script interface to VASP. This script defines a parameter called KPPRA, which automatically sets up the $k$-point mesh for similar systems. In this work, KPPRA was set to 2000, which for the primitive cells of cubic and hexagonal structures

translates to 7×7×7 and 9×9×5 $k$-point grids, respectively. The convergence tests showed that the increases of energy cutoff and $k$-points change the total energy by less than 0.01 meV.

### 2.3. Monte Carlo simulations

We adopted the conventional Monte Carlo simulations to obtain the phase diagrams of the WZ and the ZB $Cd_{1-x}Zn_xS$ alloys as well as the spatial distributions of Cd and Zn atoms in the two structures of $Cd_{0.5}Zn_{0.5}S$ alloys. We calculated their two-phase equilibrium states. In this paper, we adopted 20×20×20 and 30×30×16 supercells to calculate the phase diagrams for the WZ and the ZB $Cd_{1-x}Zn_xS$ alloys, respectively. The average time for the given precision on the average concentration of the alloy was set to 0.1% in the current simulations. A detailed description of the algorithm underlying this program can be found in Ref. [40]. The energy of the system was specified by the cluster expansion Hamiltonian. The spatial distributions of Cd and Zn atoms in $Cd_{1-x}Zn_xS$ alloys were also studied. To make the simulation feasible, we kept Cd and Zn atoms fixed at their respective lattice sites and ignore other defects.

## 3. Results and discussion

### 3.1. Ground-state structures and effective cluster interactions

In the cluster expansions of the WZ and the ZB $Cd_{1-x}Zn_xS$ alloys, 68 and 57 input structures have been used, and the CV scores are 1.3 meV and 2.3 meV, respectively. The small CV scores indicate that the predictive ability of the cluster expansions is excellent in this work. The ECIs of the WZ and the ZB $Cd_{1-x}Zn_xS$ alloys obtained from the cluster expansion are given in Table 1, and are also shown in Fig. 1. In Table 1, we adopt $J(0,1)$, $J(1,1)$, $J(2,1,\ldots,m)$, and $J(3,1,\ldots,m)$ to represent the empty, point, pair, and three-body clusters, respectively. Coordinates are in a fraction of lattice vectors. The cluster size is defined as the length of the longest pair contained in the cluster.

**Table 1.** ECIs of the wurtzite and zinc-blende $Cd_{1-x}Zn_xS$ alloys.

| Phase | Cluster | Coordinates | Size/Å | Multiplicity | ECI |
|---|---|---|---|---|---|
| WZ | $J$(0,1) | | | 1 | 0.06875 |
| | $J$(1,1) | (0.333,0.667,0.003) | | 2 | 0.00214 |
| | $J$(2,1) | (0.667,0.333,0.503) (0.333,–0.333,1.003) | 4.184 | 6 | 0.00219 |
| | $J$(2,2) | (0.667,0.333,0.503) (–0.333,–0.667,0.503) | 4.196 | 6 | 0.00440 |
| | $J$(2,3) | (0.333,0.667,0.003) (–0.333,–0.667,–0.497) | 5.925 | 6 | –0.00401 |
| | $J$(2,4) | (0.667,0.333,0.503) (-0.333,-0.667,-0.497) | 6.822 | 2 | –0.00105 |
| | $J$(2,5) | (0.333,0.667,0.003) (1.667,2.333,–0.497) | 7.268 | 6 | -0.00161 |
| | $J$(2,6) | (0.667,0.333,0.503) (–0.333,-1.667,1.503) | 9.968 | 6 | –0.00129 |
| | $J$(2,7) | (0.333,0.667,0.003) (0.667,1.333,–1.497) | 10.516 | 6 | –0.00217 |
| | $J$(2,8) | (0.333,0.667,0.003) (–1.667,–1.333,–0.997) | 10.815 | 12 | -0.00123 |
| | $J$(2,9) | (0.333,0.667,0.003) (–0.333,–1.667,–1.497) | 11.322 | 6 | –0.00056 |
| | $J$(2,10) | (0.667,0.333,0.503) (-0.667,-1.333,2.003 ) | 12.075 | 12 | –0.00033 |
| | $J$(2,11) | (0.333,0.667,0.003) (–2.333,-2.667,0.503) | 12.584 | 6 | 0.00000 |
| | $J$(2,12) | (0.333,0.667,0.003) (–1.333,–1.667,–1.497) | 13.454 | 12 | 0.00000 |
| | $J$(3,1) | (0.667,0.333,0.503) (0.333,–0.333,1.003) (–0.333,-0.667,0.503) | 4.196 | 6 | -0.00065 |
| | $J$(3,2) | (0.667,0.333,0.503) (0.333,–0.333,0.003) (–0.333,-0.667,0.503) | 4.196 | 6 | –0.00038 |
| | $J$(3,3) | (0.667,0.333,0.503) (–0.333,0.333,0.503) (–0.333,-0.667,0.503) | 4.196 | 2 | 0.00000 |
| ZB | $J$(0,1) | | | 1 | 0.12673 |
| | $J$(1,1) | (1.00,1.00,1.00) | | 4 | 0.00424 |
| | $J$(2,1) | (1.00,0.50,0.50) (1.50,0.50,0.00) | 4.191 | 24 | 0.00040 |
| | $J$(2,2) | (0.50,0.50,1.00) (1.50,0.50,1.00) | 5.927 | 12 | –0.00586 |
| | $J$(2,3) | (0.50,0.50,1.00) (1.50,1.00,1.50) | 7.259 | 48 | –0.00235 |
| | $J$(2,4) | (0.50,0.50,1.00) (1.50,0.50,0.00) | 8.382 | 24 | 0.00216 |
| | $J$(3,1) | (1.00,0.50,0.50) (1.50,0.50,0.00) (1.00,0.00,0.00) | 4.191 | 16 | -0.00122 |
| | $J$(3,2) | (1.00,0.50,0.50) (0.50,0.50,0.00) (1.00,0.00,0.00) | 4.191 | 16 | 0.00000 |

As we can see in Table 1, the cluster expansion of the WZ $Cd_{1-x}Zn_xS$ alloys includes interactions up to twelve neighboring pairs and three three-body terms to obtain the desired CV score. For the ZB $Cd_{1-x}Zn_xS$ alloys, it includes interactions of four neighboring pairs and two three-body terms to obtain the desired CV score. The presence of the three-body terms implies an asymmetric miscibility gap in the $Cd_{1-x}Zn_xS$ system.[47] It is evident that the first and the second neighboring pair ECIs for WZ and the first neighboring pair ECIs for ZB are positive, which is related to the ordering tendency of $Cd_{1-x}Zn_xS$. However, the third and the fourth neighboring pair ECIs for WZ as well as the second and the third neighboring pair ECIs for ZB are negative, which appears to counteract with the ordering tendency and is related to the tendency of

phase separation.[48,49] As shown in Fig. 1, the magnitude of ECI is reduced gradually as the distance and the cluster size increase, and the convergence is obtained ultimately.

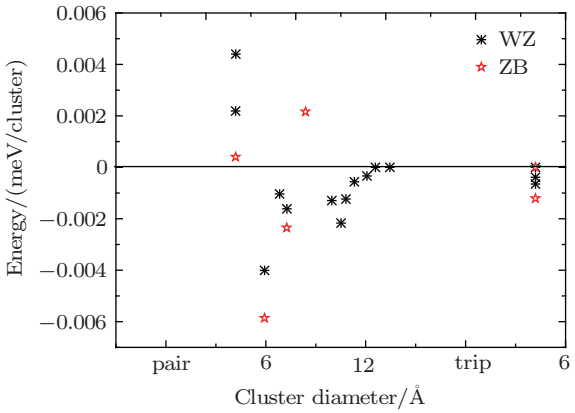



**Fig. 1.** (color online) ECIs of WZ and ZB $Cd_{1-x}Zn_xS$ alloys versus cluster diameter. The horizontal axis represents the cluster diameters; the first is for pair clusters, and the next is for triplet clusters. The cluster diameter is defined as the length of the longest pair contained in the cluster.

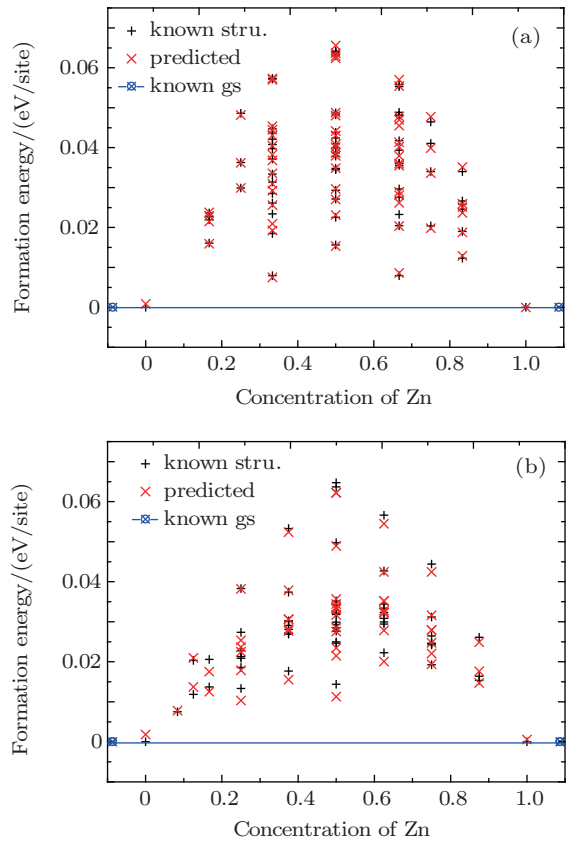



**Fig. 2.** (color online) Cluster expansion of formation energies and direct enumeration ground-state search results of $Cd_{1-x}Zn_xS$ solid solutions: (a) WZ structure, (b) ZB structure. The "known stru." denotes structures whose energies have been calculated from first-principles. The "known gs" indicates the ground states that have been confirmed by first-principles calculations. The "predicted" denotes structures whose energies have been predicted from the cluster expansion and *ab initio* energies are known.

The formation energies of WZ and ZB $Cd_{1-x}Zn_xS$ solid solutions are shown in Figs. 2(a) and 2(b), respectively. The formation energy $\Delta E_f(\sigma)$ of configuration $\sigma$ is calculated as follows:

$$\Delta E_f(\sigma) = E(\sigma) - [(1-x)E(\mathrm{CdS}) + xE(\mathrm{ZnS})], \quad (3)$$

where $E(\sigma)$ is the total energy (per cation) of a given configuration of $Cd_{1-x}Zn_xS$ solid solution, $E$(CdS) is the energy of CdS, and $E$(ZnS) is the energy of ZnS. The direct enumeration approach has been used for constructing the ground-state hull.[50] The ground states are identified as breaking points of the concentration versus energy of formation convex hull. As we can see in Figs. 2(a) and 2(b), all the formation energies are positive, which indicates that the $Cd_{1-x}Zn_xS$ solid solutions are unstable and have a tendency to decompose into two terminal phases (CdS and ZnS phases). The phase separation introduces inhomogeneity into $Cd_{1-x}Zn_xS$ alloys, which is in agreement with the experimental results.[51,52]

### 3.2. Charge transfer to S atoms

We computed the amount of charge transfer between cations and anions in each input structure of WZ and ZB $Cd_{1-x}Zn_xS$ alloys by Bader charge analysis technique.[53–55] We obtained the average amount of charge transfer to S atoms for each Zn concentration. The statistical error of the average charge transfer was too large for some concentrations with a small number of structures (less than 3), so we did not take them into consideration. As the electrons of Cd and Zn atoms transfer to S atoms in WZ and ZB $Cd_{1-x}Zn_xS$ alloys, the amount of charge gained by S atoms shows the ionicity of these alloys. As we can see in Fig. 3, the average amount of charge gained by S atoms in WZ $Cd_{1-x}Zn_xS$ alloys is higher than that in ZB $Cd_{1-x}Zn_xS$ alloys except when $x$ is 0 and 1. It indicates that the ionicity of WZ $Cd_{1-x}Zn_xS$ is stronger than that of ZB $Cd_{1-x}Zn_xS$. The average amount of charge gained by S atoms increases with the increase of the Zn concentration in the two structures. It means that the ionicity of $Cd_{1-x}Zn_xS$ alloys is stronger with the doping of Zn.

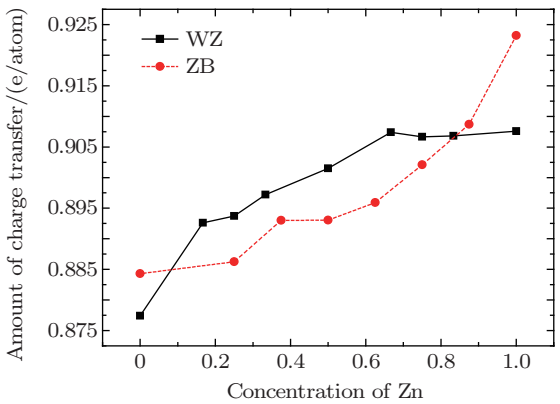



**Fig. 3.** (color online) The average amount of charge transfer to S atoms versus the Zn concentration in WZ and ZB $Cd_{1-x}Zn_xS$ alloys.

### 3.3. Phase diagram

Figure 4 shows the calculated phase diagrams of WZ and ZB $Cd_{1-x}Zn_xS$ alloys. In Fig. 4, the binodal curves correspond to the coexistence of CdS and ZnS phases. Inside the curves, the phase separation can occur thermodynamically for both the WZ and the ZB $Cd_{1-x}Zn_xS$ alloys. Outside the curves, the $Cd_{1-x}Zn_xS$ solid solutions are stable and homogenous. As shown in Fig. 4, for the WZ and the ZB $Cd_{1-x}Zn_xS$ alloys, the consolute temperatures are 655 K and 604 K, respectively, and the corresponding consolute concentrations are 0.646 and 0.695. Both binodal curves are asymmetric. The binodal curve of WZ $Cd_{1-x}Zn_xS$ we obtained is close to that of Lu *et al.*[24] Their result shows that the consolute temperature of WZ $Cd_{1-x}Zn_xS$ is 613 K, which is just 42 K lower than ours. The consolute concentration they obtained is about 0.68, and is in fair agreement with our result. It should be noted that the computational method we adopted is different from that of Lu *et al.*[24] though the results are similar. Zhang *et al.*[12] found that at the temperature of 723 K, the WZ $Cd_{1-x}Zn_xS$ solid solution can be synthesized uninterruptedly and homogenously. While at 673 K, the $Cd_{1-x}Zn_xS$ film is rough and uneven; its surface appears to exhibit the phenomenon of segregation, which is consistent with the consolute temperature of 655 K obtained by us. All of these indicate that the phase diagram of the WZ $Cd_{1-x}Zn_xS$ alloy we obtained is reliable. We have also computed the phase diagram of the ZB $Cd_{1-x}Zn_xS$ solid solutions by the same method. The calculated consolute temperature $T_c$ of the ZB $Cd_{1-x}Zn_xS$ solid solutions is 604 K, which is much lower than 1278 K obtained by Zhou *et al.*[25] Our results agree well with the experiment, as the synthesis was carried out at 513 K ($x = 0.13$ and 0.66).[56,57]

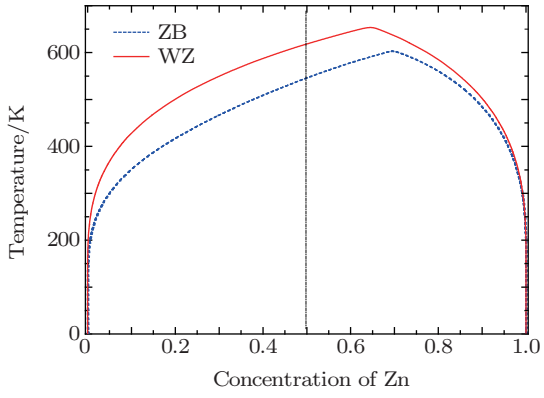



**Fig. 4.** (color online) Phase diagrams of WZ and ZB $Cd_{1-x}Zn_xS$ alloys.

### 3.4. Distributions of Cd and Zn atoms in $Cd_{1-x}Zn_xS$ alloys

We calculated the spatial distributions of Cd and Zn (active atoms) in WZ and ZB $Cd_{0.5}Zn_{0.5}S$ alloys at the temperatures of 300 K, 600 K, 650 K, 700 K and 300 K, 550 K, 600 K, 650 K, respectively. As we can see in Fig. 5, there is a phase separation in the WZ $Cd_{0.5}Zn_{0.5}S$ alloy at the temperatures of 300 K and 600 K, which means that the coexistence of CdS and ZnS phases is stable at low temperature. As the temperature increases, the alloy tends to be homogeneous, especially when the temperature is over 650 K. The ZB $Cd_{0.5}Zn_{0.5}S$ solid solution has a similar tendency as the temperature increases.

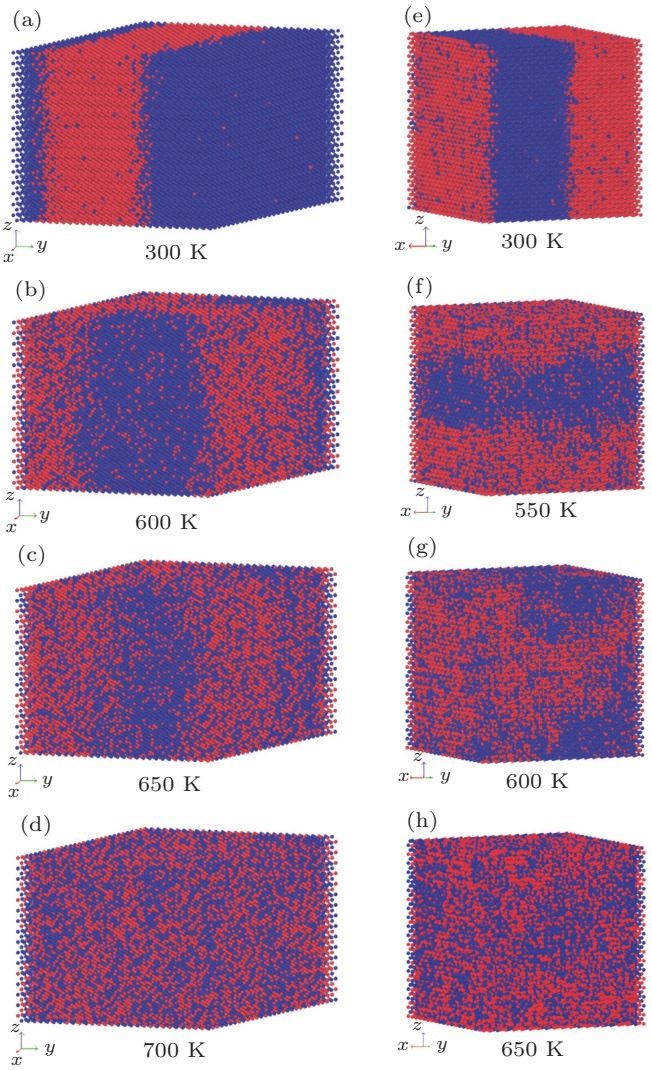



**Fig. 5.** (color online) Snapshots of (a)–(d) WZ and (e)–(h) ZB $Cd_{0.5}Zn_{0.5}S$ alloys at different temperatures. Red and blue spheres represent Zn and Cd atoms, respectively.

In order to study the spatial distributions of Cd and Zn atoms in WZ and ZB $Cd_{0.5}Zn_{0.5}S$ alloys at different temperatures quantitatively, we divided the WZ and the ZB supercells into 1800 and 2000 segments, respectively. Each segment has 16 active atoms for both WZ and ZB $Cd_{0.5}Zn_{0.5}S$ alloys. We counted the number of Cd atoms in each segment. The standard deviation $\sigma$ was computed as follows:

$$\sigma = \sqrt{\frac{1}{N}\sum_{i=1}^{N}(x_i - \bar{x})}, \tag{4}$$

where $N$ is the number of segments in the supercells, $x_i$ is the number of Cd atoms in segment $i$, and $\bar{x}$ is the average number of Cd atoms of all segments. The standard deviation $\sigma$

was used to describe the inhomogeneous degree of the spatial distribution of Cd and Zn atoms in $Cd_{0.5}Zn_{0.5}S$ alloys. The dependence of the standard deviation on temperature for WZ and ZB $Cd_{0.5}Zn_{0.5}S$ alloys is shown in Fig. 6. It is seen that the standard deviations of the two structures typically decrease with increasing temperature. It means that both WZ and ZB $Cd_{0.5}Zn_{0.5}S$ alloys become more and more homogeneous as the temperature increases. It is obvious that the standard deviations change slowly when the temperature is below 400 K, but there are abrupt changes at the range of 400 K to 650 K. There are almost no changes when the temperature is above 650 K. It means that both WZ and ZB $Cd_{0.5}Zn_{0.5}S$ alloys are inhomogeneous below 400 K, and they become homogeneous quickly above 400 K, which indicates that the $Cd_{0.5}Zn_{0.5}S$ alloys will undergo a phase transition. The degree of homogeneity is almost unchanged above 650 K.

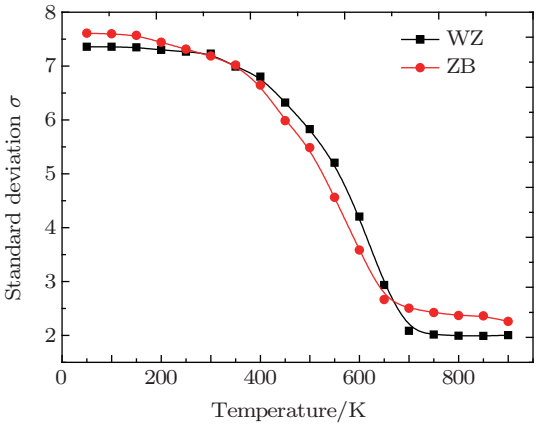



**Fig. 6.** (color online) The standard deviation $\sigma$ of WZ and ZB $Cd_{0.5}Zn_{0.5}S$ alloys as a function of temperature.

## 4. Conclusion

We obtained the phase diagrams of the wurtzite and the zinc-blende $Cd_{1-x}Zn_xS$ solid solutions by first-principles calculations based on density functional theory combined with the cluster expansion technique and Monte Carlo simulation. For the CdS–ZnS pseudobinary system, all formation energies of WZ and ZB $Cd_{1-x}Zn_xS$ alloys are positive, indicating that both WZ and ZB $Cd_{1-x}Zn_xS$ solid solutions have a tendency to phase separation. The consolute temperatures for the two structures are 655 K and 604 K, respectively, and the miscibility gaps of the two structures are asymmetric, showing a deviation toward to the higher $x$ side. The results of the spatial distributions of Cd and Zn atoms in $Cd_{0.5}Zn_{0.5}S$ alloys show that the $Cd_{1-x}Zn_xS$ alloys are inhomogeneous and exhibit a phase separation at low temperatures. The analysis of the standard deviations indicates that both WZ and ZB $Cd_{1-x}Zn_xS$ solid solutions have large inhomogeneous degrees below 400 K and rapidly become homogeneous at the temperature range of 400 K to 650 K, and their homogeneous degrees are almost unchanged above 650 K.

## Acknowledgement

This work was performed in Gansu Supercomputer Center.

## References

[1] Yamada A, Matsubara K and Sakurai K 2004 *Appl. Phys. Lett.* **85** 5607
[2] Gao X D, Li X M and Yu W D 2004 *Thin Solid Films* **468** 43
[3] Li D F, Li B L, Xiao H Y and Dong H N 2011 *Chin. Phys. B* **20** 067101
[4] Chen D S, Yang J, Xu F, Zhou P H and Du H W 2013 *Chin. Phys. B* **22** 018801
[5] Baykul M C and Orhan N 2010 *Thin Solid Films* **518** 1925
[6] Chavhan S D, Senthilarasu S and Lee S H 2008 *Appl. Surf. Sci.* **254** 4539
[7] Kumar T P, Saravanakumar S and Sankaranarayanan K 2011 *Appl. Surf. Sci.* **257** 1923
[8] Devadoss I, Muthukumaran S and Ashokkumar M 2014 *J. Mater. Sci: Mater. Electron.* **25** 3308
[9] Peter A J and Lee C W 2012 *Chin. Phys. B* **21** 087302
[10] Kokotov M and Hodes G 2010 *Chem. Mater.* **22** 5483
[11] Mariappan R, Ragavendar M and Ponnuswamy V 2011 *J. Alloys Compd.* **509** 7337
[12] Zhang T W, Zhu C J, Wang C Z and Li J 2013 *Rare Metals* **32** 47
[13] Dong Y J, Zhou L M and Wu S M 2014 *Mater. Sci. Semicond. Process.* **19** 78
[14] Hou J W, Lv X Y, Li Z H, Zou H and Zeng X F 2014 *J. Alloys Compd.* **616** 97
[15] Hetterich M, Petillon S, Petri W, Dinger A, Grün M and Klingshirn C 1996 *J. Cryst. Growth* **159** 81
[16] Borse S V, Chavhan S D and Sharma R 2007 *J. Alloys Compd.* **436** 407
[17] Akdoğan Y, Üzüm C, Dag Ö and Coombs N 2006 *J. Mater. Chem.* **16** 2048
[18] Zu S N, Wang Z Y, Liu B, Fan X P and Qian G D 2009 *J. Alloys Compd.* **476** 689
[19] Yang G R, Zhang Q, Chang W and Yan W 2013 *J. Alloys Compd.* **580** 29
[20] He X B and Gao L 2010 *J. Colloid Interface Sci.* **349** 159
[21] Jiao Z Y, Niu Y J, Shen K S and Huang X F 2014 *Mol. Phys.* **112** 1057
[22] Wan F C, Tang F L, Lu W J, Si F J, Bao H W and Xue H T 2013 *Journal of Henan University* **43** 32 (in Chinese)
[23] Wu J C, Zheng J W, Zacherl C L, Wu P, Liu Z K and Xu R 2011 *J. Phys. Chem. C* **115** 19741
[24] Lu J B, Dai Y, Guo M, Wei W, Ma Y D, Han S H and Huang B B 2012 *ChemPhysChem* **13** 147
[25] Zhou Z H, Shi J W, Wu P and Guo L J 2014 *ChemPhysChem* **15** 3125
[26] Zhou Z H, Shi J W, Wu P and Guo L J 2014 *Phys. Status Solidi B* **251** 655
[27] Sharma R C and Chang Y A 1996 *J. Phase Equilib.* **17** 425
[28] Sharma R C and Chang Y A 1996 *J. Phase Equilib.* **17** 261
[29] Stöhr M, Podloucky R and Müller S 2009 *J. Phys.: Condens. Matter* **21** 134017
[30] Liu B, Seko A and Tanaka I 2012 *Phys. Rev. B* **86** 245202
[31] Li X K, Xue H T, Tang F L and Lu W J 2015 *Mater. Sci. Semicond. Process.* **39** 96
[32] Xue H T, Tang F L, Li X K, Wan F C, Lu W J, Rui Z Y and Feng Y D 2014 *Mater. Sci. Semicond. Process.* **25** 251
[33] Ludwig C D R, Gruhn T and Felser C 2010 *Phys. Rev. Lett.* **105** 025702
[34] Sanchez J M, Ducastelle F and Gratias D 1984 *Physica A* **128** 334
[35] Lu Z W, Wei S H, Zunger A, Frota-Pessoa S and Ferreira L G 1991 *Phys. Rev. B* **44** 512
[36] Zunger A, Wang L G, Hart G L W and Sanati M 2002 *Modell. Simul. Mater. Sci. Eng.* **10** 685
[37] Sanchez J M 2010 *Phys. Rev. B* **81** 224202
[38] Ravi C, Sahu H K, Valsakumar M C and Van de Walle A 2010 *Phys. Rev. B* **81** 104111
[39] Van de Walle A, Asta M and Ceder G 2002 *Calphad* **26** 539

[40] Van de Walle A and Asta M 2002 *Modell. Simul. Mater. Sci. Eng.* **10** 521
[41] Van de Walle A and Ceder G 2002 *J. Phase Equilib.* **23** 348
[42] Kresse G and Hafner J 1993 *Phys. Rev. B* **47** 558
[43] Kresse G and Furthmuller J 1996 *Phys. Rev. B* **54** 11169
[44] Blöchl P E 1994 *Phys. Rev. B* **50** 17953
[45] Kresse G and Joubert D 1999 *Phys. Rev. B* **59** 1758
[46] Perdew J P, Burke K and Ernzerhof M 1996 *Phys. Rev. Lett.* **77** 3865
[47] Adjaoud O, Steinle-Neumann G, Burton B P and Van de Walle A 2009 *Phys. Rev. B* **80** 134112
[48] Blum V and Zunger A 2004 *Phys. Rev. B* **70** 155108
[49] Blum V and Zunger A 2005 *Phys. Rev. B* **72** 020104
[50] Ferreira L G, Wei S H and Zunger A 1991 *Int. J. High Perform. Comput. Appl.* **5** 34
[51] Zhong X H, Feng Y Y, Knoll W and Han M Y 2003 *J. Am. Chem. Soc.* **125** 13559
[52] Tosun B S, Pettit C, Campbell S A and Aydil E S 2012 *ACS Appl. Mater. Interfaces* **4** 3676
[53] Tang W, Sanville E and Henkelman G 2009 *J. Phys.: Condens. Matter* **21** 084204
[54] Sanville E, Kenny S D, Smith R and Henkelman G 2007 *J. Comput. Chem.* **28** 899
[55] Henkelman G, Arnaldsson A and Jónsson H 2006 *Comput. Mater. Sci.* **36** 354
[56] Ouyang J Y, Ripmeester J A, Wu X H, Kingston D, Yu K, Joly A G and Chen W 2007 *J. Phys. Chem. C* **111** 16261
[57] Ouyang J Y, Ratcliffe C I, Kingston D, Wilkinson B, Kuijper J, Wu X H, Ripmeester J A and Yu K 2008 *J. Phys. Chem. C* **112** 4908